Evidence for Kinetic Nucleation in Helical Nanofiber Formation Directed by Chiral Solvent for a Perylene Bisimide Organogelator

ARTICLE *in* CHEMISTRY - A EUROPEAN JOURNAL · MARCH 2013

Impact Factor: 5.73 · DOI: 10.1002/chem.201204146 · Source: PubMed

4 AUTHORS, INCLUDING:

Vladimir Stepanenko
University of Wuerzburg
65 PUBLICATIONS **2,051** CITATIONS

SEE PROFILE

CHEMISTRY
A EUROPEAN JOURNAL

ChemPubSoc
Europe

DOI: 10.1002/chem.201204146

VIP

Evidence for Kinetic Nucleation in Helical Nanofiber Formation Directed by Chiral Solvent for a Perylene Bisimide Organogelator

Vladimir Stepanenko, Xue-Qing Li, Jana Gershberg, and Frank Würthner*[a]

Abstract: The self-assembly behavior of an achiral perylene bisimide (PBI) organogelator that bears two 3,4,5-tridodecyloxybenzoylaminoethyl substituents at the imide positions has been investigated in chiral solvents (*R*)- and (*S*)-limonene in great detail by circular dichroism (CD) spectroscopy and atomic force microscopy (AFM). CD spectroscopic studies on dilute solutions revealed a preferential population of one-handed helical assemblies in chiral solvent with an enantiomeric excess close to 100%, whereas AFM images of more than 100 nanofibers of the organogel obtained from more concentrated solutions were found to consist of both handed helices with an enantiomeric excess of only 20%. This discrepancy is attributed to the fast gelation process at high dye concentration that evidently proceeds through non-equilibrated nuclei in a kinetic rather than thermodynamic self-assembly process. Under these conditions the chiral induction from the homochiral solvent may not be adequate in effectively populating only one-handed helices.

Keywords: chirality · dyes/pigments · organogels · self-assembly · supramolecular chirality

Introduction

Helical architectures such as DNA and proteins are ubiquitous in nature and they are appreciated by chemists for their structural as well as functional features.[1] The design of helical architectures is accordingly of great interest for chemists. Over the past decade, various noncovalent interactions, such as hydrogen bonding, metal-ion to ligand coordination, electrostatic interactions, π–π stacking, dipole–dipole interactions, hydrophobic interactions, and so forth, have been identified for the generation of self-assembled architectures based on synthetic small molecule building blocks.[2] A significant number of those architectures are self-assembled helical nanofibers that were obtained from chiral building blocks by virtue of noncovalent interactions.[3] Likewise, helical nanofibers and chiral supramolecular structures have been observed upon self-assembly of achiral molecular building blocks.[3c,4] However, such chiral self-assembled nanofibers composed of achiral building blocks are commonly a mixture of both left- and right-handed helices in equal amounts, and thus the systems are overall racemic.[5,6] Although some examples can be found in the literature that describe the purposive selection of one-handed helicity by symmetry breaking at a primary state of nucleation, for example, by vortex motion,[7,8] it remains a critical issue that the experimental evidence of these studies relies on bisignate CD signals, which, according to more recent work, may also result from the macroscopic alignment of extended fibers by vortex effects.[9,10] In a less disputable experiment, supramolecular helicity is induced by chiral solvents or by chiral additives.[11] For instance, Kirstein and co-workers observed that a carbocyanine dye forms optically active superhelical J-aggregates in aqueous solution in the presence of a chiral alcohol.[11a] This indicates the possibility of preferential population of one-handed helices by external chiral bias imparted by a suitable chiral solvent.

In our previous work, we have demonstrated that achiral amide-functionalized perylene bisimides (**PBI 1** in Figure 1) self-assemble into one-dimensional helical nanofibers by synergic effects of π–π stacking and hydrogen-bonding interactions.[12a] In some apolar solvents, such as toluene, the fine fibers further intercross to form three-dimensional network structures, by which the solvents are immobilized resulting in organogels. Atomic force microscopy (AFM) studies revealed that the fibrous aggregates of **PBI 1** exhibit a highly defined helical pitch, and the left- and right-handed helices appear in equal amounts. Furthermore, we have shown that chiral derivative **PBI 2** self-assembles exclusively into nanofibers with single-handed helicity according to AFM microscopy.[13] These results suggest that even small helical bias as imparted by chiral substituents at peripheral positions can direct the self-assembly process of these molecules into nanofibers of single-handed helicity.

In a comprehensive study, we have elucidated the impact of different achiral and chiral substituents for **PBIs 1–3** and four more derivatives on the helical bias of their fibrous aggregates by CD spectroscopy and AFM, and analyzed the self-sorting capabilities of mixtures composed of those dyes.[14] In this work, we report our results on the impact of external chiral bias exerted by a homochiral solvent on the

[a] Dr. V. Stepanenko, Dr. X.-Q. Li, J. Gershberg, Prof. Dr. F. Würthner
Universität Würzburg, Institut für Organische Chemie
and Center for Nanosystems Chemistry
Am Hubland, 97074 Würzburg (Germany)
Fax: (+49) 931-31-84756
E-mail: wuerthner@chemie.uni-wuerzburg.de

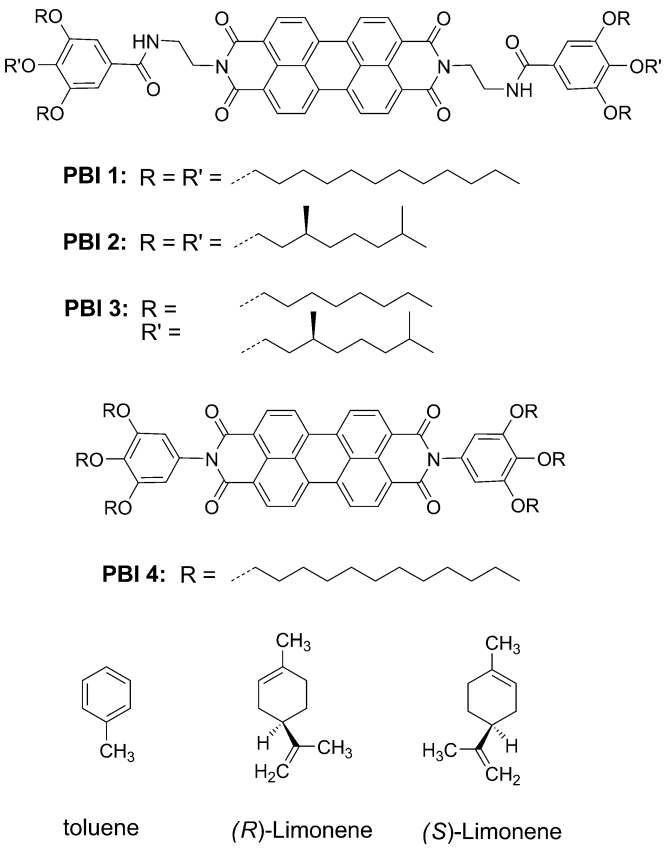

Figure 1. Molecular structures of **PBI 1–4** and solvent molecules applied in this study.

helicity of the aggregates of achiral **PBI 1**. Based on the careful analysis of the helicity of more than 100 nanofibers by AFM, we were able to quantitatively interpret the observed CD effects and to show that the formation of **PBI 1** organogels[15] proceeds through a non-equilibrium self-assembly, that is, by a kinetic nucleation process.[16]

Figure 1 depicts the molecular structures of benzoylamide-functionalized **PBIs 1–3** as well as a reference **PBI 4** that lacks the amide groups required for hydrogen bonding. According to our previous studies, the amide functional groups assist the face-to-face π–π stacking of the PBI cores with a rotational displacement of about 30°,[17] as found for **PBI 2**.[13] More importantly, by means of additional amide–amide hydrogen bonds, the rotational displacement is fixed in a single handedness to give an extended helical nanofiber that is sufficiently robust for the gelation of organic solvents at lowest concentrations.[12a] In contrast, no gelation phenomena are observed in any solvents for **PBI 4** due to the much smaller aggregate size in the absence of hydrogen-bonding ability.

Results and Discussion

Self-assembly and gelation properties: Self-assembly of **PBI 1** was investigated by UV/Vis spectroscopy. Figure 2a and b show the temperature-dependent UV/Vis spectra of **PBI 1** in (*R*)- and (*S*)-limonene, respectively. The degree of aggregation of **PBI 1** in limonene can be easily adjusted by changing the temperature at a certain concentration. The absorption spectra of **PBI 1** in (*R*)- and (*S*)-limonene are almost identical to those observed in temperature-dependent studies in toluene,[12a] that is, at high temperatures of approximately 100 °C the characteristic vibronic pattern for monomeric PBI dyes is observed with a $\lambda_{max} = 522$ nm, whereas at low temperatures of approximately 35 °C a typical aggregate spectrum is observed with a blueshifted absorption maximum and a reduced absorption strength. According to exciton coupling theory, such hypsochromic shifts (H-band) can be attributed to a sandwich-type packing of the chromophores. A second less intense J-band around 545 nm of the aggregate spectrum indicates rotational displacements, that is, a helical packing of the PBI chromophores. Identical spectral features were observed for **PBI 1**

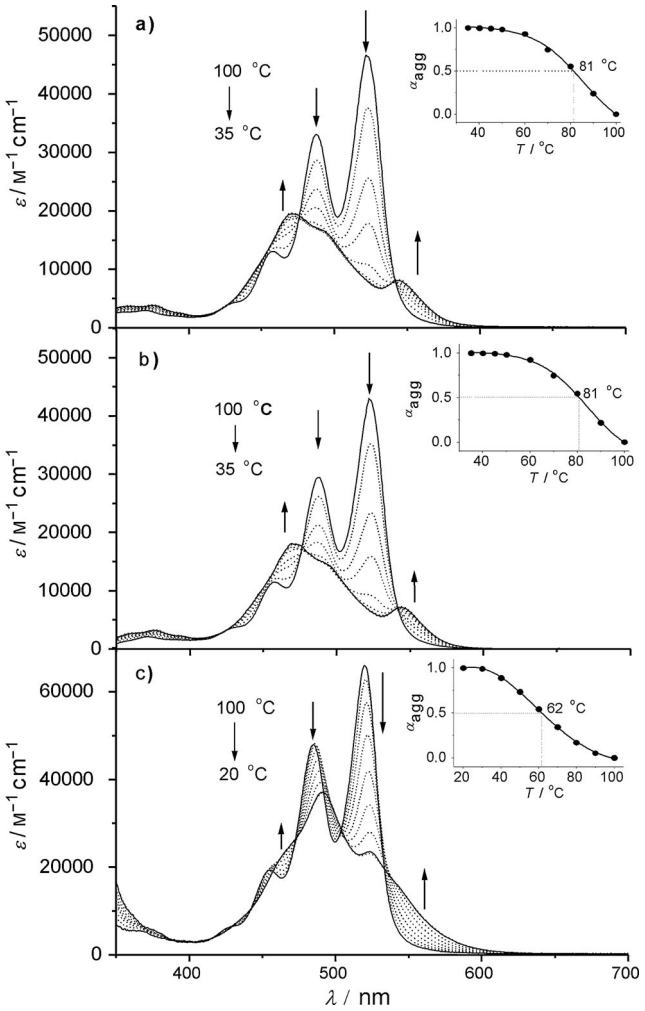

Figure 2. Temperature-dependent UV/Vis absorption spectra of a) **PBI 1** in (*R*)-limonene (5.1×10^{-5} M), b) **PBI 1** in (*S*)-limonene (5.0×10^{-5} M), and c) **PBI 4** in (*R*)-limonene (5.0×10^{-5} M). The arrows indicate spectral changes with decreasing temperature. Insets show the plots of α_{agg} as a function of temperature. The sigmoidal fits for the data points were obtained by using the Boltzmann function.

in (*R*)- and (*S*)-limonene, suggesting equal propensity of aggregate formation in both enantiomers of apolar limonene solvent.

For comparison, Figure 2c shows the variable-temperature absorption spectra of **PBI 4** in (*R*)-limonene. At high temperature the dye molecules prevail as non-aggregated monomers, which is reflected by a characteristic monomer absorption band. Upon cooling, π–π stacking takes place with a decrease of the absorption coefficient at $\lambda_{max} = 520$ nm (monomer), a concomitant blueshift of the absorption maximum and a pronounced shoulder at longer wavelength of around 560 nm. These spectral features are indicative of the typical face-to-face stacking mode of perylene bisimide species with rotationally displaced chromophores.[17,18]

Notably, the π–π stacking of **PBI 1** starts at considerably lower concentration (5×10^{-8} M, in both (*R*)- and (*S*)-limonene) at room temperature, which is attributed to the assistance by hydrogen-bond formation. In contrast, the self-assembly of reference **PBI 4** requires a higher concentration of about 1×10^{-6} M in (*R*)-limonene, because of the inefficient strength of π–π stacking in the absence of hydrogen bonding. Note that the critical gelation concentration of **PBI 1** in (*R*)- and (*S*)-limonene is far higher, that is, 0.8×10^{-3} M.

Insets in Figure 2 show the mole fraction of aggregate at each temperature estimated by using Equation (1) in which $\alpha_{agg}(T)$ is the mole fraction of aggregated dye at temperature T, A_{mon}, $A(T)$ and A_{agg} are the absorbance (taken at 522 nm) for the monomer, the solution at temperature T and the pure aggregate solutions, respectively.

$$\alpha_{agg}(T) \approx \frac{A(T)-A_{mon}}{A_{agg}-A_{mon}} \quad (1)$$

The $\alpha_{agg}(T)$ values were plotted as a function of temperature and fitted by using the Boltzmann function. From such a plot the α_{50} (T) (temperature at which $\alpha_{agg}=0.5$) could be estimated. As indicated in the insets of Figure 2a–c, the α_{50} value of **PBI 1** was determined as 81 °C in (*R*)- and (*S*)-limonene, which is higher than that of **PBI 4** in (*R*)-limonene (62 °C). The significantly higher α_{50} values of **PBI 1** again confirms the higher binding strength of this building block due to additional hydrogen bonds.

While the UV/Vis spectroscopic studies delivered information on the intermolecular coupling of the π-systems' transition dipole moments, structural evidence was obtained by AFM. Unlike **PBI 4** and other structurally similar PBI derivatives, which adopt short achiral rod-like aggregates,[19] **PBI 1** forms more extended fibers with defined helicity that further intercross to network structures in apolar solvents. Figure 3 shows the AFM images of a diluted **PBI 1** gel in toluene, in which well-defined long fibers (several microns in length) and 3D network structures are observed. The mean height of the helical fibers was (3.1±0.3) nm with a width of (8.0±2.0) nm and a helical pitch of (15.0±2.0) nm. The fine fibers can further assemble into broad ropes with width varying from 20 to 80 nm.

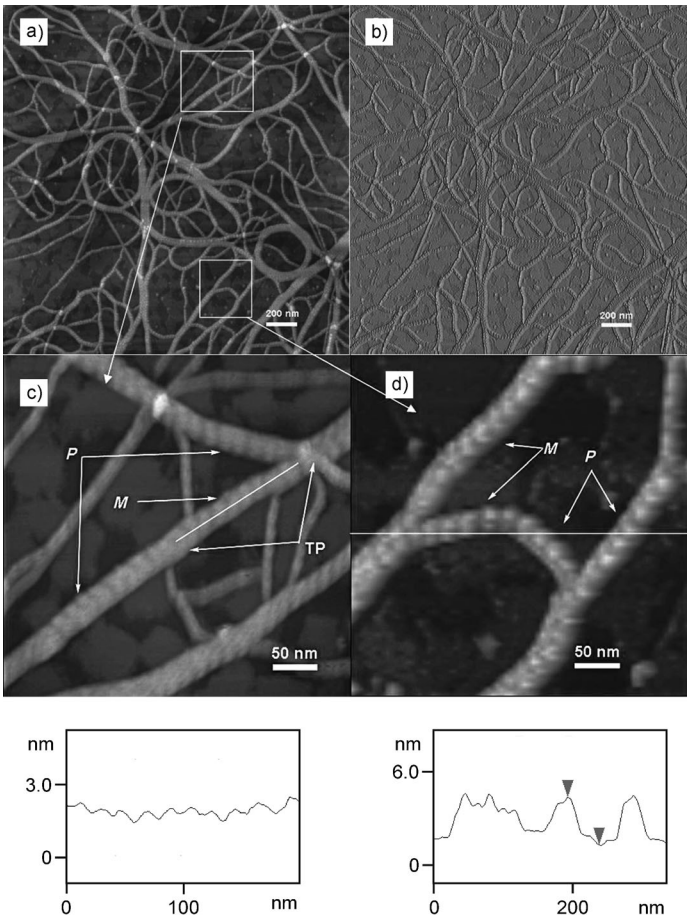

Figure 3. AFM a) height and b) phase images of films spin-coated from a diluted gel solution of **PBI 1** in toluene ($c=1\times10^{-4}$ M) on HOPG surface; c) and d) are zoomed region images from a); bottom figures show the cross-section analyses corresponding to the white lines of c) and d), respectively. The scale bars in a) and b) are 200 nm, and those in c) and d) are 50 nm.

The zoomed images show that the fibers adopt clear helicities and both left- (*M*) and right-handed (*P*) helices can be found simultaneously in the present network matrix. Note that there is no preference for the handedness of helices and that even conversion points are observed in a single fiber (the transition points are labeled as "TP" in Figure 3c).

The well-defined helical pitch of these nanofibers can be explained by hydrogen-bond-directed π–π stacking. Molecular modeling studies (Figure 4) show the two mirror image possibilities for the hydrogen-bond-directed chromophore packing into *M*- and *P*-helical π stacks. Considering that the precursors are intrinsically achiral, it is reasonable that the two enantiomeric π stacks should be present in equal amounts in an achiral environment. The two hydrogen-bonding "pillars" are highlighted to play an important role in the formation of helicity, because they can efficiently direct single-handed helical sense (see enlarged area in Figure 4). In contrast, for simple PBI π stacks without such hydrogen-bonding functionality the helical sense can easily change within a π stack, because of equal interaction ener-

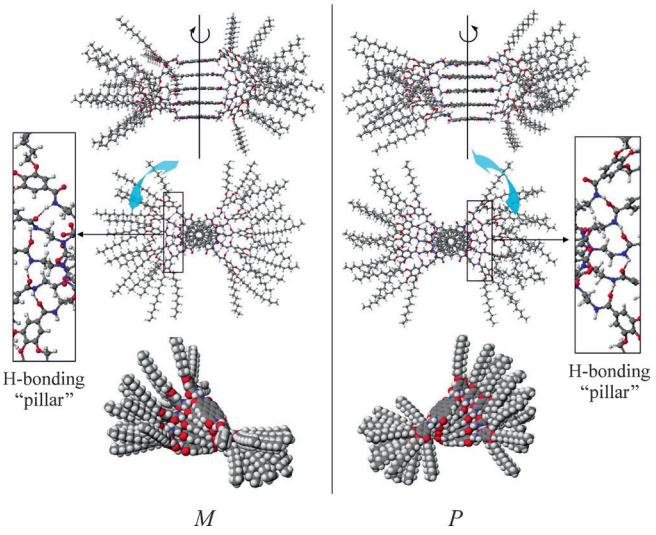

Figure 4. Suggested packing models for self-assembled *P*- and *M*-configured hydrogen-bonded aggregates of **PBI 1**. The enlarged area shows the hydrogen-bond pillars formed between the amide groups. Atom assignment: gray: carbon; white: hydrogen; red: oxygen; blue: nitrogen.

gies between individual *M*- or *P*-configured co-facially stacked PBI dimeric units.[18a,20]

CD studies on helical bias by chiral solvents: The network formed by **PBI 1** in toluene comprises well-organized helical fibers and bundles; however, the whole material is racemic, which is reasonable, since the building blocks and the exterior environment are achiral. This situation changes when the peripheral alkyl chains of **PBI 1** are replaced by chiral analogues, for example, **PBI 2**.[13,14] Another source of chiral bias might be provided by chiral solvents. To explore this scope, we have chosen chiral (*R*)- and (*S*)-limonene (see Figure 1 for structures) as they exhibit chirality centers and their structures are similar to methylcyclohexane and toluene, in which the self-assembly of the **PBI 1** chromophore has been intensively studied before.[12a]

To monitor the helical arrangement of the chromophores upon self-assembly, temperature-dependent CD spectroscopic studies were carried out in (*R*)- and (*S*)-limonene, respectively (Figure 5a). At elevated temperature no Cotton effect was observed as expected for monomeric **PBI 1**. When the temperature was decreased, concomitant with the formation of self-assembled PBI stacks (see Figure 2) a significant induced bisignate Cotton effect was observed with a positive maximum at 458 nm and a negative maximum at 499 nm. We assume that the observed CD spectra are attributable to thermodynamically equilibrated aggregates, because identical spectra could be recorded at the respective temperatures upon heating and cooling. In addition, a second negative maximum was observed at 546 nm corresponding to the lowest energy exciton band of the UV/Vis spectrum (Figure 2a). The shape and intensity ($\Delta\varepsilon_{max}$ of ca. 50 $M^{-1}cm^{-1}$) of the CD spectra appears similar to those observed for PBI chromophores with chiral side chains,[14]

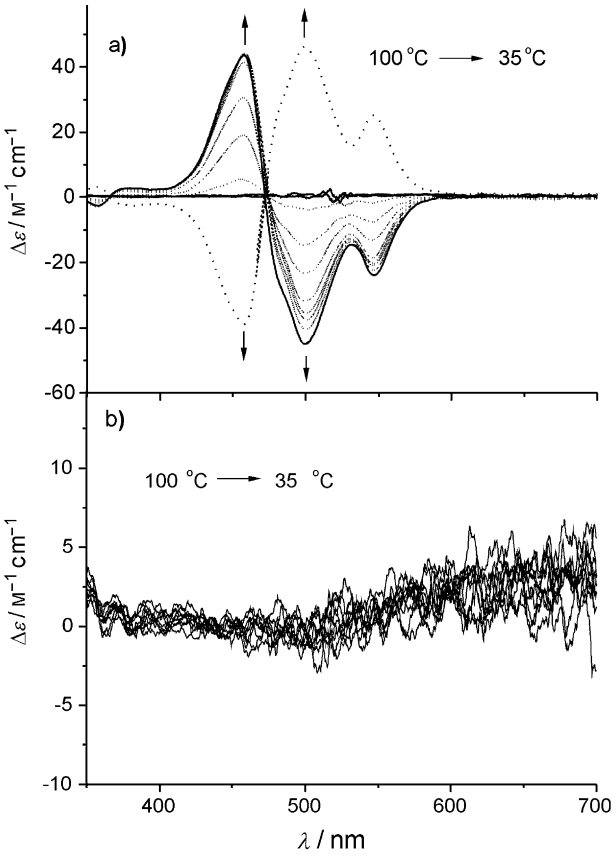

Figure 5. Temperature-dependent CD spectra of a) **PBI 1** in (*R*)-limonene (solid lines, 5.0×10^{-5} M) and (*S*)-limonene (dotted line, 5.0×10^{-5} M) and b) **PBI 4** in (*R*)-limonene (5.1×10^{-5} M). For all measurements the equilibrating time between each spectrum was approximately 18 min. Under these conditions, identical spectra were recorded upon heating and cooling at a given temperature. Arrows indicate the spectral changes upon decreasing the temperature from 100 °C to 35 °C.

which suggests a comparable helical bias imparted by the chiral side chain and the chiral solvent. The bisignate shape of the CD spectra in (*R*)-limonene (solid lines, Figure 5) indicates the preferential formation of left-handed (*M*-configured) π-stacks according to the exciton chirality method.[21]

When similar temperature-dependent studies were carried out in (*S*)-limonene, the observed CD spectra were perfect mirror images of those found in the case of (*R*)-limonene (Figure 5a, dotted line: 458 nm, negative; 499 nm, positive; 546 nm, positive), which indicate a right-handed (*P*-configured) helicity of the aggregates. The observation of reversed CD spectra of **PBI 1** in (*R*)- and (*S*)-limonene reveals that the chiral environment directs the helical sense of the chromophore packing, which results in a chiral bias towards homochiral aggregates.

For comparison, the solution of reference **PBI 4** in (*R*)-limonene was cooled in a similar fashion and the CD spectra were monitored. Unlike gelator **PBI 1**, in this case no Cotton effect could be observed upon cooling, although aggregation took place under this condition as indicated by the UV/Vis spectra (Figure 2c). Thus, in the absence of additional "pillars" formed by hydrogen bonding the rotational

offset upon co-facial stacking of PBIs cannot be directed to a preferential helicity by the external chiral environment.

AFM studies on nanofiber chirality: For an analysis of the helicity of **PBI 1** nanofibers by AFM, more extended aggregates are needed. Such nanofibers are formed only at higher concentration upon cooling of hot solutions leading to organogels. Accordingly, gels were prepared from a 1×10^{-4} M solution of **PBI 1** in either (*S*)- or (*R*)-limonene. In our typical procedure the solution is heated until the dye molecules are dissolved homogenously. Subsequently, the solution is allowed to cool down to about 50 °C, from which it is spin-coated on highly oriented pyrolytic graphite (HOPG) with a spinning rate of 2000 rpm. Thus the increase of concentration and cooling take place simultaneously, leading to well-defined and elongated nanofibers. The AFM images of gels formed in (*S*)-limonene are shown in Figure 6. Two types of fibers can be recognized: without and with helicity (labeled as 1 and 2, respectively, in Figure 6b). The smaller fibers without helicity on HOPG have only a height of (1.2 ± 0.1) nm. These structures are pretty rare and might be the result of a **PBI 1** self-assembly process that is directed by the template effect of HOPG due to the well-known strong interactions between alkyl chains and this substrate. The height of the more abundant, larger helical structures is (2.6 ± 0.2) nm and the mean helical pitch is (19.0 ± 1.0) nm. Thus, both values are very similar to those found for **PBI 1** nanofibers prepared from toluene (see Figure 3). Whilst CD spectroscopic studies revealed a preferential population of one-handed helices in chiral solvents (Figure 5), they do not provide any quantitative information on the enantiomeric excess. In contrast, AFM images of the gels with well-resolved helicity can provide this information although such analysis has been rarely performed.[22] At first glance, the **PBI 1** gels formed in (*S*)-limonene were found to consist of both types of helices. However, close inspection of the left-handed (*M*) and right-handed (*P*) helicity in large-scale AFM image in Figure 6a revealed 51 legible helical fibers, 30 right-handed (*P*) ones populate a majority of 59% and 21 left-handed (*M*) ones populate a minority of 41% as shown in the statistical graph of Figure 6.

AFM studies were also performed on **PBI 1** nanofibers formed upon gelation in (*R*)-limonene. As shown in Figure 7, similar network structures can be observed as in (*S*)-limonene with micrometer length and defined helicities, in which both *M* and *P* configurations are adopted. Conversely to the case in (*S*)-limonene, 36 helical fibers in Figure 7a suggest a left-handed helical sense domination (58%), whilst only 26 (42%) are right-handed. Thus, we can conclude from our AFM analysis that the enantiomeric excess (*ee*) of the more abundant chiral fibers is around 20% in organogels formed in (*R*)- or (*S*)-limonene.

The excess of *P*-configured helical fibers upon spin-coating from (*S*)-limonene and *M*-configured helical fibers from (*R*)-limonene observed in AFM is qualitatively in accordance with the observed helical bias in solution recorded by CD spectroscopy. However, quantitatively the helical bias of the **PBI 1** nanofibers towards a single handedness was less

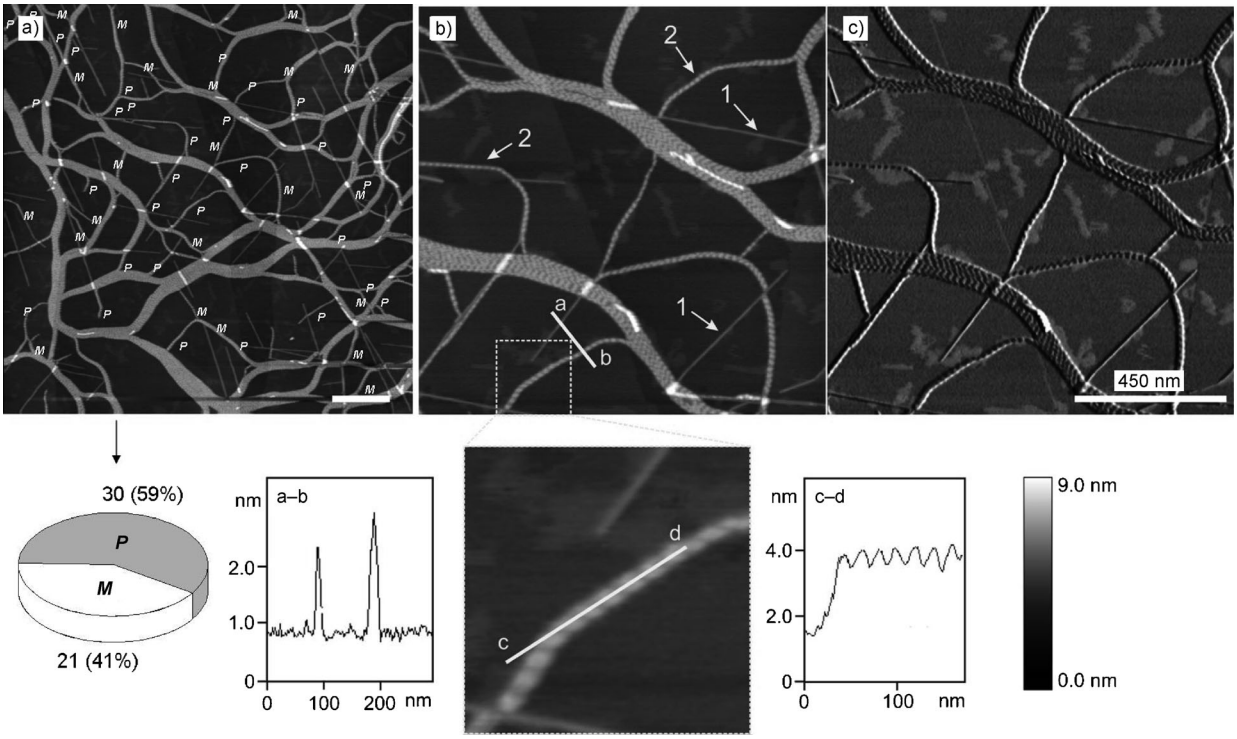

Figure 6. AFM images of a film spin-coated (2000 rpm) from a solution of **PBI 1** in (*S*)-limonene ($c=1\times10^{-4}$ M) onto HOPG. a) and b): Height images. c): Phase image. The scale bars in a) and c) correspond to 450 nm, the *z* scale in a) and b) is 9 nm. The statistical graph of *M* and *P* helices is derived from image a). a–b and c–d are cross-section analyses of the fibers.

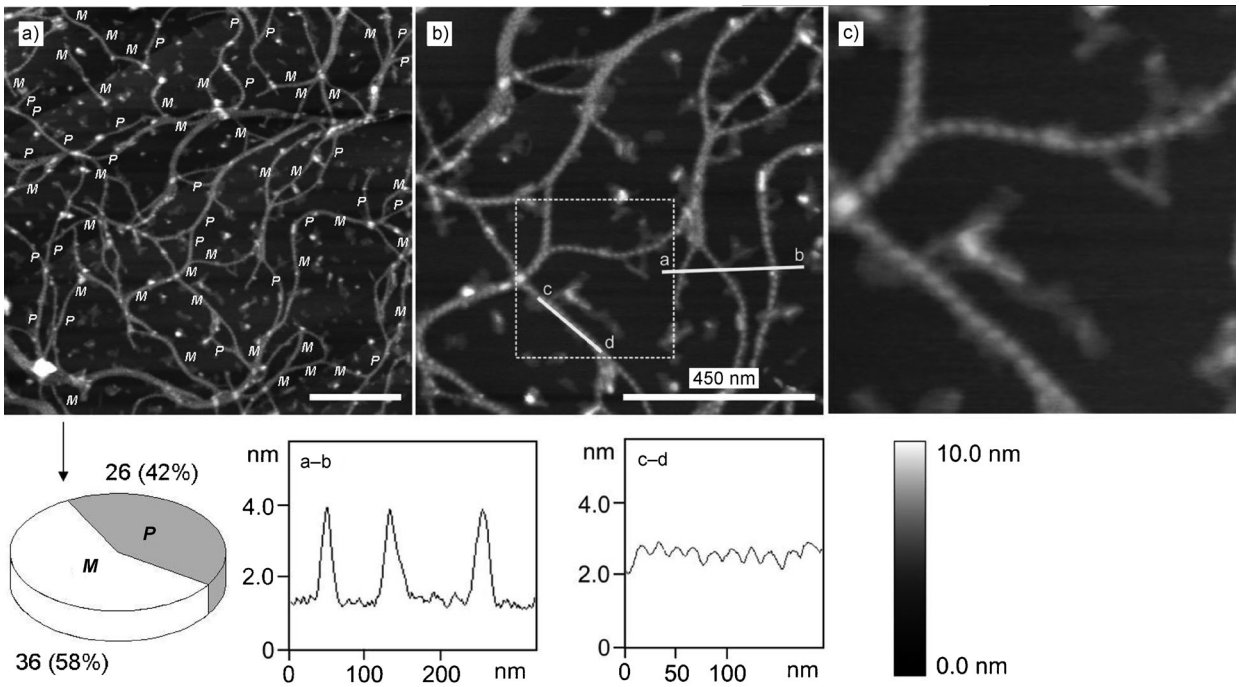

Figure 7. AFM images of a film spin-coated (2000 rpm) from a solution of **PBI 1** in (*R*)-limonene ($c=1\times10^{-4}$ M) onto HOPG. The scale bar of a) and b) is 450 nm, the *z* scale is 10 nm. c) is zoomed region image of b). The statistical graph of *M* and *P* helices is derived from image a). a–b and c–d are cross-section analyses of the fibers.

pronounced than expected. For the structurally related organogelator **PBI 2** bearing six chiral aliphatic side chains, single-handed helices were found upon spin-coating from achiral solvents according to AFM studies.[13] Interestingly, however, again fibers of both handednesses were observed upon spin-coating from achiral solvents for another structurally related chiral organogelator, that is, **PBI 3**, that is equipped with only two chiral aliphatic side chains (R') indicating a weaker influence of the chiral centers (no statistical analysis has been performed in this case).[14] These results point at a subtle effect of the remote chiral centers, being either of internal (=chiral substituent) or external (=chiral solvent) origin, on the chiral nucleus from which the single-handed helical fibers grow.

Whilst the small-sized aggregates observed by CD experiments at low concentrations between 10^{-6} and 10^{-5} M are thermodynamically equilibrated (see above), the situation may be different for the organogel samples formed at higher concentrations upon cooling. Under these conditions, the gelation is a pretty instantaneous process (fast cooling rate, high dye concentration) and accordingly the process of chiral induction from the solvent may be governed by kinetic effects.[16] This intuitive explanation is in accordance with recent kinetic investigations by Meijer and co-workers on self-assembly pathways of chiral oligo(*p*-phenylenevinylene-s)[16a] that revealed the influence of concentration and temperature on the competing kinetic and thermodynamic self-assembly pathways.

To confirm the formation of kinetically trapped **PBI 1** assemblies, a solution of **PBI 1** (1.0×10^{-4} M) in (*R*)-limonene, prepared under the same conditions as previous AFM studies, was cooled down from 100 to 20 °C at different cooling rates (Figure 8). When cooled at slow rates of 80 °C h^{-1}, an intense bisignate CD signal was recorded ($\Delta\varepsilon_{max}$ ca. $-33\,M^{-1}cm^{-1}$ at $\lambda=506$ nm). Notably, this value is still smaller, by about 30%, than the value obtained upon slow cooling of more dilute solutions in which smaller-sized aggregates prevail (Figure 5). When the cooling rate was further increased, the CD signals became weaker. At the fastest accessible cooling rate with our instrumentation (300 °C h^{-1}), we observed a decrease of the CD amplitude to $\Delta\varepsilon_{max}$ of approximately $-22\,M^{-1}cm^{-1}$, while fast cooling outside the instrument led to an even smaller CD signal of $\Delta\varepsilon_{max}$ of roughly $-12\,M^{-1}cm^{-1}$ at $\lambda=506$ nm (Figure 8a). These results suggest the formation of kinetically trapped nuclei which exhibit a smaller enantiomeric excess upon fast cooling. Because the cooling rate in our gelation experiment is supposed to be similar to the fastest cooling CD experiment, we may conclude that the smaller than expected helical bias found in our AFM analysis is an outcome of a gelation process governed by kinetic self-assembly.

According to our AFM analyses in the fast cooling regime an *ee* of 20% was achieved. This value can now be related to the observed CD spectra in the fastest cooling experiment. Thus, an $\Delta\varepsilon_{max}$ value of $12\,M^{-1}cm^{-1}$ (at $\lambda=506$ nm) corresponds an *ee* of 20%. From Equation (2), we can now calculate the expected $\Delta\varepsilon_{max}$ value for enantiopure nanofibers to be $60\,M^{-1}cm^{-1}$.

$$ee = \Delta\varepsilon_{obs}/\Delta\varepsilon_{max} \times 100 \quad (2)$$

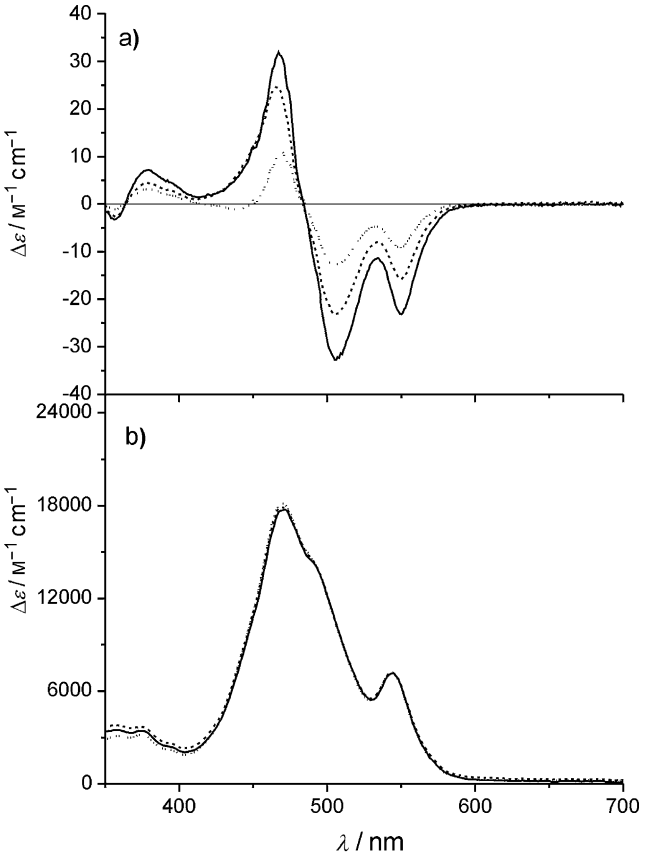

Figure 8. a) Cooling speed dependent CD spectra and b) corresponding UV/Vis absorptions spectra of **PBI 1** (1.0×10^{-4} M) in (*R*)-limonene. The sample was cooled from 100 to 20 °C at rates of 80 (solid line) and 300 °C h^{-1} (dashed line), and rapid cooling outside the instrument to 20 °C after preparing the sample (dotted line).

Most pleasingly, within the experimental error of CD spectroscopy and our statistical AFM analyses, this value corresponds acceptably to the observed CD values measured for small aggregates of **PBI 1** at the lower concentration of 5.0×10^{-5} M in (*R*)- or (*S*)-limonene at slow cooling rates ($\Delta\varepsilon_{max}$ ca. 47 M^{-1}cm^{-1} at $\lambda = 506$ nm, see Figure 5). This suggests the formation of almost homochiral aggregates in dilute solution upon slow cooling, that is, under thermodynamic control.

Conclusion

In this paper, we have investigated the impact of chiral solvents on the self-assembly of achiral **PBI 1** molecules by UV/Vis and CD spectroscopy as well as atomic force microscopy. In solution, **PBI 1** molecules form long helical fibers by π–π stacking and hydrogen-bonding interactions. In achiral solvent such as toluene, both left- and right-handed helices co-exist in equal amounts and the system is overall chiroptically silent. However, in chiral environment the *M*/*P* ratio is biased and a preferential helicity can be selected by choosing a chiral solvent, such as (*R*)- or (*S*)-limonene. Under thermodynamic conditions (low concentration, sufficient equilibration time) the helical bias appears to be almost quantitative for **PBI 1** in (*R*)- or (*S*)-limonene (*ee* close to 100 %). The fact that the helical bias was less pronounced (*ee* = 20 %) for organogel fibers formed at higher concentration according to the analysis of more than 100 helical fibers by AFM could be explained by a fast nucleation and growth process into extended fibers during the gelation process, which leads to kinetic rather than thermodynamic self-assembly products. It is very likely that many, if not the majority of reported organogels are formed through non-equilibrated nuclei that rapidly grow into extended aggregate structures during the fast cooling process at rather high substrate concentrations.

Experimental Section

Materials and methods: All solvents and reagents were purchased from commercial sources. The solvents for spectroscopic studies were of spectroscopic grade and used as received. (*R*)- and (*S*)-limonene were purchased from Merck. **PBI 1** and **PBI 4** were synthesized as described previously.[12a,18b]

UV/Vis and CD spectroscopy: UV/Vis spectra were measured in a Perkin–Elmer Lambda 950 spectrometer equipped with a Peltier system as temperature controller. All the solutions were measured in conventional quartz cell of 0.1 cm to 1 cm path length to cover a suitable concentration range. The CD spectra were recorded with a Jasco J-810 spectropolarimeter equipped with Jasco CDF 426S temperature controller. All the solutions were measured in conventional quartz cell of 1 cm path length.

Atomic force microscopy (AFM): AFM measurements were performed under ambient conditions using a Bruker AXS MultiMode Nanoscope IV system operating in tapping mode in air. Silicon cantilevers (OMCL-AC160TS) with a resonance frequency of approximately 300 kHz and a spring constant of roughly 42 N m^{-1} were used. For AFM studies, the gels were prepared from a 1×10^{-4} M solution of **PBI 1** in either (*S*)- or (*R*)-limonene. To ensure a defined starting point, that is, monomeric PBI dyes, the samples were heated until all dyes were completely dissolved and the UV/Vis absorption bands showed the characteristic vibronic patterns of monomeric species. The solution was then allowed to cool to a temperature of about 50 °C, from which it was spin-coated on highly oriented pyrolytic graphite (HOPG) with a rotating speed of 2000 rpm.

Acknowledgements

This work was financially supported by the Deutsche Forschungsgemeinschaft (Grant no: Wu 317/15-1).

[1] a) J. J. L. M. Cornelissen, A. E. Rowan, R. J. M. Nolte, N. A. J. M. Sommerdijk, *Chem. Rev.* **2001**, *101*, 4039–4070; b) M. Albrecht, *Chem. Rev.* **2001**, *101*, 3457–3497; c) K. R. MacKenzie, *Chem. Rev.* **2006**, *106*, 1931–1977; d) C. Schmuck, *Angew. Chem.* **2003**, *115*, 2552–2556; *Angew. Chem. Int. Ed.* **2003**, *42*, 2448–2452.
[2] a) F. M. Hoeben, P. Jonkheijm, E. W. Meijer, A. P. H. J. Schenning, *Chem. Rev.* **2005**, *105*, 1491–1546; b) D. González-Rodríguez, A. P. H. J. Schenning, *Chem. Mater.* **2011**, *23*, 310–325.
[3] a) T. Shimizu, M. Masuda, H. Minamikawa, *Chem. Rev.* **2005**, *105*, 1401–1443; b) L. A. Estroff, A. D. Hamilton, *Chem. Rev.* **2004**, *104*, 1201–1217; c) C. C. Lee, C. Grenier, E. W. Meijer, A. P. H. J. Schenning, *Chem. Soc. Rev.* **2009**, *38*, 671–683.

[4] a) A. R. A. Palmans, J. A. J. M. Vekemans, E. E. Havinga, E. W. Meijer, *Angew. Chem.* **1997**, *109*, 2763–2765; *Angew. Chem. Int. Ed. Engl.* **1997**, *36*, 2648–2651; b) G. Dantlgraber, A. Eremin, S. Diele, A. Hauser, H. Kresse, G. Pelzl, C. Tschierske, *Angew. Chem.* **2002**, *114*, 2514–2518; *Angew. Chem. Int. Ed.* **2002**, *41*, 2408–2412; c) M. R. Molla, A. Das, S. Ghosh, *Chem. Commun.* **2011**, *47*, 8934–8936.

[5] M. Suarez, N. Branda, J.-M. Lehn, A. Decian, J. Fischer, *Helv. Chim. Acta* **1998**, *81*, 1–13.

[6] W. Yang, X. Chai, L. Chi, X. Liu, Y. Cao, R. Lu, Y. Jiang, X. Tang, H. Fuchs, T. Li, *Chem. Eur. J.* **1999**, *5*, 1144–1149.

[7] a) U. De Rossi, S. Dähne, S. C. J. Meskers, H. P. J. M. Dekkers, *Angew. Chem.* **1996**, *108*, 827–830; *Angew. Chem. Int. Ed. Engl.* **1996**, *35*, 760–763; b) A. Pawlik, S. Kirstein, U. De Rossi, S. Dähne, *J. Phys. Chem. B* **1997**, *101*, 5646–5651; c) C. Spitz, S. Dähne, *J. Phys. Chem. B* **2000**, *104*, 8664–8669; d) S. Kirstein, H. von Berlepsch, C. Böttcher, C. Burger, A. Ouart, G. Reck, S. Dähne, *ChemPhysChem* **2000**, *1*, 146–150.

[8] a) J. M. Ribó, J. Crusats, F. Sagues, J. M. Claret, R. Ruvires, *Science* **2001**, *292*, 2063–2066; b) R. Rubires, J.-A. Farrera, J. M. Ribó, *Chem. Eur. J.* **2001**, *7*, 436–446.

[9] a) A. Tsuda, Md. A. Alam, T. Harada, T. Yamaguchi, N. Ishii, T. Aida, *Angew. Chem.* **2007**, *119*, 8346–8350; *Angew. Chem. Int. Ed.* **2007**, *46*, 8198–8202; b) M. Wolffs, S. J. George, Ž. Tomović, S. C. J. Meskers, A. P. H. J. Schenning, E. W. Meijer, *Angew. Chem.* **2007**, *119*, 8351–8353; *Angew. Chem. Int. Ed.* **2007**, *46*, 8203–8205; c) G. P. Spada, *Angew. Chem.* **2008**, *120*, 646–648; *Angew. Chem. Int. Ed.* **2008**, *47*, 636–638; d) A. Tsuda, Y. Nagamine, R. Watanabe, Y. Nagatani, N. Ishii, T. Aida, *Nat. Chem.* **2010**, *2*, 977–983; e) Y. Ando, T. Sugihara, K. Kimura, A. Tsuda, *Chem. Commun.* **2011**, *47*, 11748–11750.

[10] a) M. Eriksson, M. Härdelin, A. Larsson, J. Bergenholtz, B. Åkerman, *J. Phys. Chem. B* **2007**, *111*, 1139–1148; b) U. Pindur, M. Jansen, T. Lemster, *Curr. Med. Chem.* **2005**, *12*, 2805–2847.

[11] a) H. von Berlepsch, S. Kirstein, C. Böttcher, *J. Phys. Chem. B* **2003**, *107*, 9646–9654; b) J. Aimi, Y. Nagamine, A. Tsuda, A. Muranaka, M. Uchiyama, T. Aida, *Angew. Chem.* **2008**, *120*, 5231–5234; *Angew. Chem. Int. Ed.* **2008**, *47*, 5153–5156; c) Y. Zhang, P. Chen, M. Liu, *Chem. Eur. J.* **2008**, *14*, 1793–1803; d) S. J. George, Z. Tomović, A. P. H. J. Schenning, E. W. Meijer, *Chem. Commun.* **2011**, *47*, 3451–3453; e) for a review on chiral amplification phenomena, see A. R. A. Palmans, E. W. Meijer, *Angew. Chem.* **2007**, *119*, 9106–9126; *Angew. Chem. Int. Ed.* **2007**, *46*, 8948–8968.

[12] a) X.-Q. Li, V. Stepanenko, Z. Chen, P. Prins, L. D. A. Siebbeles, F. Würthner, *Chem. Commun.* **2006**, 3871–3873; for related helical nanofibers formed by hydrogen-bond-assisted π–π stacking of perylene bisimides and homologous naphthalene bisimides, see: b) B. Jancy, S. K. Asha, *Chem. Mater.* **2008**, *20*, 169–181; c) N. B. Kolhe, R. N. Devi, S. P. Senanayak, B. Jancy, K. S. Narayan, S. K. Asha, *J. Mater. Chem.* **2012**, *22*, 15235–15246; d) M. R. Molla, S. Ghosh, *Chem. Mater.* **2011**, *23*, 95–105; e) M. R. Molla, A. Das, S. Ghosh, *Chem. Eur. J.* **2010**, *16*, 10084–10093; f) A. Das, M. R. Molla, B. Maity, D. Koley, S. Ghosh, *Chem. Eur. J.* **2012**, *18*, 9849–9859.

[13] F. Würthner, C. Bauer, V. Stepanenko, S. Yagai, *Adv. Mater.* **2008**, *20*, 1695–1698.

[14] S. Ghosh, X.-Q. Li, V. Stepanenko, F. Würthner, *Chem. Eur. J.* **2008**, *14*, 11343–11357.

[15] For reviews on organogels, see: a) S. S. Babu, S. Prasanthkumar, A. Ajayaghosh, *Angew. Chem.* **2012**, *124*, 1800–1810; *Angew. Chem. Int. Ed.* **2012**, *51*, 1766–1776; b) T. Ishi-I, S. Shinkai, *Top. Curr. Chem.* **2005**, *258*, 119–160; c) A. Brizard, R. Oda, I. Huc, *Top. Curr. Chem.* **2005**, *256*, 167–218; d) U. Beginn, *Prog. Polym. Sci.* **2003**, *28*, 1049–1105.

[16] a) P. A. Korevaar, S. J. George, A. J. Markvoort, M. M. J. Smulders, P. A. J. Hilbers, A. P. H. J. Schenning, T. F. A. De Greef, E. W. Meijer, *Nature* **2012**, *481*, 492–496; b) Y. Tidhar, H. Weissman, S. G. Wolf, A. Gulino, B. Rybtchinski, *Chem. Eur. J.* **2011**, *17*, 6068–6075; c) A. Lohr, F. Würthner, *Isr. J. Chem.* **2011**, *51*, 1052–1066; d) E. T. Pashuck, S. I. Stupp, *J. Am. Chem. Soc.* **2010**, *132*, 8819–8821; e) A. Lohr, F. Würthner, *Angew. Chem.* **2008**, *120*, 1252–1256; *Angew. Chem. Int. Ed.* **2008**, *47*, 1232–1236; for seminal works of G. M. Withesides and D. N. Reinhoudt on kinetically stable hydrogen-bonded assemblies, see: f) J. P. Mathias, E. E. Simanek, C. T. Seto, G. M. Withesides, *Angew. Chem.* **1993**, *105*, 1848–1850; *Angew. Chem. Int. Ed. Engl.* **1993**, *32*, 1766–1769; g) J. P. Mathias, C. T. Seto, E. E. Simanek, G. M. Withesides, *J. Am. Chem. Soc.* **1994**, *116*, 1725–1736; h) L. J. Prins, E. E. Neuteboom, V. Paraschiv, M. Crego-Calama, P. Timmerman, D. N. Reinhoudt, *J. Org. Chem.* **2002**, *67*, 4808–4820.

[17] R. Fink, J. Seibt, V. Engel, M. Renz, M. Kaupp, S. Lochbrunner, H.-M. Zhao, J. Pfister, F. Würthner, B. Engels, *J. Am. Chem. Soc.* **2008**, *130*, 12858–12859.

[18] a) F. Würthner, C. Thalacker, S. Diele, C. Tschierske, *Chem. Eur. J.* **2001**, *7*, 2245–2253; b) Z. Chen, U. Baumeister, C. Tschierske, F. Würthner, *Chem. Eur. J.* **2007**, *13*, 450–465; c) Z. Chen, B. Fimmel, F. Würthner, *Org. Biomol. Chem.* **2012**, *10*, 5845–5855.

[19] V. Dehm, Z. Chen, U. Baumeister, P. Prins, L. D. A. Siebbeles, F. Würthner, *Org. Lett.* **2007**, *9*, 1085–1088.

[20] M. R. Hansen, T. Schnitzler, W. Pisula, R. Graf, K. Müllen, H. W. Spiess, *Angew. Chem.* **2009**, *121*, 4691–4695; *Angew. Chem. Int. Ed.* **2009**, *48*, 4621–4624.

[21] N. Berova, K. Nakanishi, R. W. Woody, *Circular Dichroism: Principles and Applications*, Wiley-VCH, Weinheim, **2000**.

[22] AFM for statistical analysis, see S. Sakurai, S. Ohsawa, K. Nagai, K. Okoshi, J. Kumaki, E. Yashima, *Angew. Chem.* **2007**, *119*, 7749–7752; *Angew. Chem. Int. Ed.* **2007**, *46*, 7605–7608.

Received: November 20, 2012
Published online: February 11, 2013

